

Equilibrium model prediction for the scatter in the star-forming main sequence

Sourav Mitra^{1*}, Romeel Davé^{1,2,3}, Vimal Simha¹, Kristian Finlator⁴

¹ *University of the Western Cape, Bellville, Cape Town 7535, South Africa*

² *South African Astronomical Observatories, Observatory, Cape Town 7925, South Africa*

³ *African Institute for Mathematical Sciences, Muizenberg, Cape Town 7945, South Africa*

⁴ *New Mexico State University, Las Cruces, NM, USA*

1 March 2022

ABSTRACT

The analytic “equilibrium model” for galaxy evolution using a mass balance equation is able to reproduce mean observed galaxy scaling relations between stellar mass, halo mass, star formation rate (SFR) and metallicity across the majority of cosmic time with a small number of parameters related to feedback. Here we aim to test this data-constrained model to quantify deviations from the mean relation between stellar mass and SFR, i.e. the star-forming galaxy main sequence (MS). We implement fluctuation in halo accretion rates parameterised from merger-based simulations, and quantify the intrinsic scatter introduced into the MS under the assumption that fluctuations in star formation follow baryonic inflow fluctuations. We predict the $1\text{-}\sigma$ MS scatter to be $\sim 0.2\text{--}0.25$ dex over the stellar mass range $10^8 M_\odot$ to $10^{11} M_\odot$ and a redshift range $0.5 \lesssim z \lesssim 3$ for SFRs averaged over 100 Myr. The scatter increases modestly at $z \gtrsim 3$, as well as by averaging over shorter timescales. The contribution from merger-induced star formation is generally small, around 5% today and 10 – 15% during the peak epoch of cosmic star formation. These results are generally consistent with available observations, suggesting that deviations from the MS primarily reflect stochasticity in the inflow rate owing to halo mergers.

Key words: galaxies: formation, galaxies: evolution, galaxies: abundances, galaxies: mass function

1 INTRODUCTION

Over the past few years, advances in large multi-wavelength galaxy surveys have considerably increased our knowledge of galaxy evolution. In particular, such surveys have served to greatly constrain the scaling relations between global galaxy properties, which places constraints on the nature of galaxy growth. As observational uncertainties, both statistical and systematic, are lowered, key galaxy scaling relations have been shown to be quite tight, such as the relationship between stellar mass and gas-phase metallicity that shows a scatter of ~ 0.1 dex or less (Tremonti et al. 2004). These scaling relations suggest an underlying simplicity involved in the various complex processes of galaxy evolution.

A particularly well-investigated scaling relation is that between the star formation rate (SFR) and stellar mass (M_*) in star-forming galaxies (SFGs), colloquially known as the SFG “main sequence” (MS). The MS extends over several orders of magnitudes in M_* and out to high redshifts, with a modest scatter of ~ 0.3 dex (Noeske et al. 2007; Elbaz et al. 2007; Daddi et al. 2007; Salim

et al. 2007; Whitaker et al. 2012; Schreiber et al. 2015) which includes both intrinsic scatter and measurement uncertainties. The existence of such tight scatter at all observed epochs suggests that most galaxies assembled their stellar mass fairly steadily rather than predominantly in starburst episodes, implying that mergers have a sub-dominant contribution to the global star formation history (Rodighiero et al. 2011; Sargent et al. 2012; Schreiber et al. 2015).

Concurrently, cosmological simulations highlighted the fact that the inflow of gas fueling star formation into galaxies enters predominantly in smooth, cold accretion (Kereš et al. 2005; Dekel et al. 2009). However, it has long been recognised that unabated accretion would result in galaxies far too large compared to observations (White & Frenk 1991; Balogh et al. 2001), and solving this so-called “overcooling problem” requires strong feedback to suppress star formation. The now-ubiquitous observations of galactic outflows in SFGs over much of cosmic time (Martin 2005; Weiner et al. 2009; Steidel et al. 2010; Rubin et al. 2014) suggests that such outflows are the primary mechanism for self-regulation in SFGs, by ejecting copious amounts of gas from galaxies that would otherwise form into stars. Simulations now routinely include such outflow processes in order to achieve good agreement with basic

* E-mail: hisourav@gmail.com

galaxy demographics (Di Cintio et al. 2014; Genel et al. 2014; Muratov et al. 2015; Schaye et al. 2015; Somerville & Davé 2015; Davé et al. 2016; Christensen et al. 2016; Wetzel et al. 2016). Furthermore, models argue that the return of some outflow material, often called “wind recycling”, is also an important component of inflow required to match galaxy properties (e.g. Oppenheimer et al. 2010; Henriques et al. 2013). Thus it appears that, within the well-constrained growth of large-scale structure, the *baryon cycling* processes of inflows, outflows, and wind recycling govern the growth of galaxies across cosmic time.

While the physical mechanisms and dynamics require complex cosmologically-based simulations to fully describe, it is possible to obtain intuitive insights and robust constraints on baryon cycling processes using a simple analytic framework. The essential equation balances the gas inflow rate into the interstellar medium (ISM) of galaxies, versus the sum of the mass outflow rate and star formation rate, as well as fluctuations in the gas reservoir. Such models are commonly referred to as “equilibrium” (Finlator & Davé 2008; Davé et al. 2012), “gas regulator” (Lilly et al. 2013; Peng & Maiolino 2014), or “bathtub” (Bouché et al. 2010; Dekel & Mandelker 2014) models. Finlator & Davé (2008) crucially pointed out that simulations predict that the rate of change of the gas reservoir is small compared to the other terms, and setting this term exactly to zero results in simplifications that make the model more intuitive and insightful, while still being a realistic description of galaxy growth averaged over cosmological timescales. We call this assumption of a non-evolving gas reservoir the “equilibrium assumption,” from which the equilibrium model follows (Davé et al. 2012). Notably, the gas regulator model does not make this assumption. Regardless, this simple framework is able to capture the essential baryon cycling processes analytically, thereby enabling a more intuitive view of how galaxy growth proceeds.

The next step in such models was to constrain the free parameters associated with baryon cycling. In Mitra et al. (2015), hereafter Paper I, we parameterised the equilibrium model with three variables corresponding to ejective feedback via a mass loading factor (η), preventive feedback via an evolving halo mass scale for quenching (ζ), and wind recycling via a typical recycling time for ejected material to re-accrete (t_{rec}). For each variable, we postulated simple dependences on halo mass and redshift, along with an overall amplitude, resulting in 9 free parameters. We found that our null hypothesis of a halo mass quenching scale of $\approx 10^{12} M_{\odot}$ at $z = 0$ was preferred by the Bayesian evidence, which reduced our number of free parameters by one. With these 8 free parameters, we then fit to observations of the stellar mass–halo mass relation, the MS, and the mass-metallicity relation from $z = 0 - 2$, using a Monte Carlo Markov Chain (MCMC) algorithm. We obtained a best-fit reduced $\chi^2 = 1.6$ to all the data at all those epochs, which is significantly better than is typically obtained in simulations or semi-analytic models (Somerville & Davé 2015). This demonstrates that the baryon cycling framework in the equilibrium model can provide a good description of galaxy growth, and moreover provides meaningful constraints on the baryon cycling variables themselves.

Our equilibrium model results suggest that one can fit the mean galaxy scaling relations and their cosmological evolution without explicitly including mergers. Nonetheless, mergers add stochasticity to galaxy evolution that was not accounted for in the Mitra et al. (2015) model. In that sense, Paper I reflects a *first order* model for galaxy evolution which only accounts for the mean evolution of the scaling relations. Meanwhile, the scatter around the mean scaling relations are driven by other processes such as

environment and the fluctuations in the inflow rate owing to mergers (Davé et al. 2011; Mitra et al. 2015; Goerdt et al. 2015). Such processes thus can be regarded as yielding *second order* deviations from the mean relations.

In this paper, we provide a quantitative test of the earlier first order equilibrium model by investigating the variations around mean trends in the main sequence. Our basic aim is to see how the inflow fluctuations, predicted from a merger-tree based approach, can give rise to observed scatter in the MS. Other groups have likewise investigated this (Dutton et al. 2010; Forbes et al. 2014; Sparre et al. 2015b; Rodríguez-Puebla et al. 2016), generally finding 0.1 – 0.4 dex scatter in the stellar mass range $10^9 M_{\odot}$ to $10^{11} M_{\odot}$, but have not done so within a MCMC-constrained equilibrium model-type framework as we do here.

This paper is structured as follows. In the next section, we review the key features of our basic equilibrium model along with the modifications made for the purpose of this work, and present the (minor) updates to the parameter constraints when including inflow fluctuations. We then present the resulting scatter in MS obtained from our model and compare it with the present observations in Section 3. Finally, we summarize and conclude our main findings in Section 4.

2 MODEL DESCRIPTION

2.1 First order model

We begin by summarizing the main features of the basic equilibrium model, built on a simple set of equations which well approximates galaxy evolution in full hydrodynamic simulations (Finlator & Davé 2008). Unlike SAMs, these models are not based on halo merger trees, nor do they attempt to track the formation of a disk and subsequent mergers, as in traditional galaxy formation theory (White & Frenk 1991; Mo et al. 1998). Instead, we rely on the view that galaxies grow along a slowly-evolving equilibrium between accretion, feedback, and star formation as outlined in Finlator & Davé (2008); Bouché et al. (2010); Davé et al. (2012); Lilly et al. (2013):

$$\dot{M}_{\text{in}} = \dot{M}_{\text{out}} + \text{SFR}, \quad (1)$$

where \dot{M}_{in} is the mass inflow rate onto the galaxy’s star-forming region and \dot{M}_{out} is outflow rate. This is a simple mass balance equation with an extra assumption that the net change of gas mass within the ISM is zero (i.e. the equilibrium assumption; Finlator & Davé 2008; Krumholz & Dekel 2012; Tacconi et al. 2013; Saito et al. 2013). From this it is possible to derive the equations for the star formation rate and metallicity within the ISM as (see Davé et al. 2012 and Mitra et al. 2015 for details):

$$\text{SFR} = \frac{\zeta \dot{M}_{\text{grav}} + \dot{M}_{\text{recyc}}}{1 + \eta}, \quad (2)$$

and

$$Z_{\text{ISM}} = \frac{y \text{SFR}}{\zeta \dot{M}_{\text{grav}}}, \quad (3)$$

where \dot{M}_{grav} is the gravitational-driven inflow of dark matter halos that is an outcome of Λ CDM cosmology, y is the metal yield, and \dot{M}_{recyc} is accretion rate of the material that was previously ejected in outflows. The above relations contain three unknown variables: η (mass loading factor or the ejective feedback parameter), ζ (preventive feedback) and t_{rec} (wind recycling time or the recycling

parameter) which are collectively known as *baryon cycling parameters* (Davé et al. 2012).

Despite ongoing efforts and improvements, the baryon cycling parameters remain difficult to constrain observationally, because inflows and outflows generally occur in diffuse, multi-phase circum-galactic gas which is challenging to fully characterise via either absorption or emission probes. The equilibrium model, instead, provides a way to constrain these parameters from the global demographic evolution of the galaxy population, within the context of the baryon cycling paradigm. To do so, we represent them by 8 free variables that quantify their behavior with halo masses and redshifts (Mitra et al. 2015):

$$\eta = \left(\frac{M_h}{10^{\eta_1 + \eta_2 \sqrt{z}}} \right)^{\eta_3} \quad (4)$$

$$t_{\text{rec}} = \tau_1 \times 10^9 \text{yr} \times (1+z)^{\tau_2} \left(\frac{M_h}{10^{12}} \right)^{\tau_3} \quad (5)$$

$$\zeta_{\text{quench}} = \text{MIN} \left[1, \left(\frac{M_h}{M_q} \right)^{\zeta_1} \right], \frac{M_q}{10^{12} M_\odot} = (0.96 + \zeta_2 z), \quad (6)$$

where ζ_{quench} is quenching feedback parameter and M_q is the quenching mass. We then employ a Bayesian MCMC approach using recent measurements of three well-known galaxy scaling relations that relate the halo mass, stellar mass, SFR and metallicity of galaxies: (i) the stellar mass (M_*) vs. halo mass (M_h) (SMHM) relation (Behroozi et al. 2013; Moster et al. 2013), (ii) the stellar mass vs. gas-phase metallicity (MZR) relation (Andrews & Martini 2013; Zahid et al. 2014; Steidel et al. 2014; Sanders et al. 2015) and (iii) the stellar mass vs. SFR relation (Speagle et al. 2014; Whitaker et al. 2014; Schreiber et al. 2015). To properly represent the evolution of the galaxy population, we consider these relations over a significant fraction of cosmic time, at redshifts $z = 0$ (today), 1 (~ 6 Gyr ago), and 2 (~ 10 Gyr ago). We refer the reader to Paper I for a detailed description of this analysis method. The only modification we make here is that, now we compute the \dot{M}_{grav} from simulations in a different way (discussed later in this section), rather than what we used earlier (i.e. a simple fitting formula from Dekel et al. 2009).

We show the match between those scaling relations and our best-fit model predictions in Figure 1 by solid black lines, which are quite similar to what we obtained in Figure 2 of Paper I, shown in dashed lines. Note that, all the error bars here reflect 1- σ or 68% confidence limits (C.L.) around the mean. The agreement is again quite good, with an overall reduced chi-squared value of ≈ 2 . The best-fit values and 68% C.L. for all 8 parameters are listed in Table 1. The results from Paper I are also shown here for comparison, which are again comparable to what we obtain here. We use the Bayesian evidence to ensure that removing any one of these 8 parameters is not statistically favored. Overall, neither hydrodynamic simulations nor SAMs employing many more parameters are able to achieve such a good match across such a wide a range of redshifts. Note that up till now, we have not explicitly considered the scatter around the scaling relations, and instead we only aim to fit the mean trends. As such, we refer to this as the *first order* equilibrium model for galaxy evolution. In the next section, we shall see how one can get a reasonable scatter in M_* -SFR relation from the fluctuations of inflow rates using a simple probabilistic approach.

| Parameters | Best-fit value and 1- σ errors | |
|------------|---------------------------------------|-------------------------|
| | This paper | Paper I |
| η_1 | $10.85^{+0.06}_{-0.06}$ | $10.98^{+0.07}_{-0.10}$ |
| η_2 | $0.81^{+0.07}_{-0.07}$ | $0.62^{+0.07}_{-0.06}$ |
| η_3 | $-1.15^{+0.08}_{-0.07}$ | $-1.16^{+0.06}_{-0.06}$ |
| τ_1 | $1.12^{+0.37}_{-0.24}$ | $0.52^{+0.24}_{-0.07}$ |
| τ_2 | $-0.62^{+0.11}_{-0.21}$ | $-0.32^{+0.06}_{-0.20}$ |
| τ_3 | $-0.47^{+0.05}_{-0.06}$ | $-0.45^{+0.10}_{-0.07}$ |
| ζ_1 | $-0.45^{+0.07}_{-0.07}$ | $-0.49^{+0.07}_{-0.08}$ |
| ζ_2 | $0.51^{+0.15}_{-0.17}$ | $0.48^{+0.13}_{-0.12}$ |

Table 1. MCMC results from first order model: best-fit values and 68% confidence limits on the all eight parameters for this paper and our Paper I.

2.2 New features

We now discuss the additional features of our model which we have implemented in this work to generate the scatter in halo accretion rate. To do so, we now need to consider the fact that the accretion of material into halos is not smooth, but rather arrives in lumps. For the dark matter, this corresponds to halo merging, which we can express using an analytical fitting formula for the dimensionless mean merger rate, $dN_m/d\epsilon dz$, where ϵ is the merger mass ratio $M_{\text{subhalo}}/M_{\text{parent}}$ (Fakhouri et al. 2010):

$$\frac{dN_m}{d\epsilon dz}(M, \epsilon, z) = A \left(\frac{M}{10^{12} M_\odot} \right)^\alpha \epsilon^\beta \exp\left(\frac{\epsilon}{\bar{\epsilon}}\right)^\gamma (1+z)^\eta. \quad (7)$$

The free parameters A , $\bar{\epsilon}$, α , β , γ and η are obtained by fitting to an N-body simulation based on Millennium (Springel et al. 2005) and Millennium-II (Boylan-Kolchin et al. 2009) simulation, but with a cosmology consistent with Planck Collaboration et al. (2015). The best-fit values are $(A, \bar{\epsilon}, \alpha, \beta, \gamma, \eta) = (0.0104, 0.00972, 0.133, -1.995, 0.263, 0.0993)$.

The cumulative number of mergers received by a halo of mass M , of objects with mass between $M_{\epsilon_{\text{min}}}$ and $M_{\epsilon_{\text{max}}}$, between redshift z_0 and z , is then given by:

$$N_m = \int_{z_0}^z dz \int_{\epsilon_{\text{min}}}^{\epsilon_{\text{max}}} d\epsilon \frac{dN_m}{d\epsilon dz}(M, \epsilon, z), \quad (8)$$

and

$$\frac{dM}{dz} = \int_{\epsilon_{\text{min}}}^{\epsilon_{\text{max}}} M \epsilon d\epsilon \frac{dN_m}{d\epsilon}(M, \epsilon, z), \quad (9)$$

from which the mass accretion rate \dot{M}_h can be calculated by a transformation of variables from redshift z to time t . This allows us to compute the baryonic inflow rate as $\dot{M}_{\text{grav}} = f_b \dot{M}_h$. We choose $\epsilon_{\text{min}} = 10^4 M_\odot / M_{\text{parent}}$, thereby capturing all mergers down to $M_h = 10^4 M_\odot$. We have tested our model with different limits of ϵ_{min} and although the “smooth” component (discussed below) changes a bit, the overall results remain the same.

For a halo of mass M , we compute the number of mergers received in some time interval dt in bins of mass ratio ϵ using equation 8. We then sample the distribution of N_m as a function of ϵ

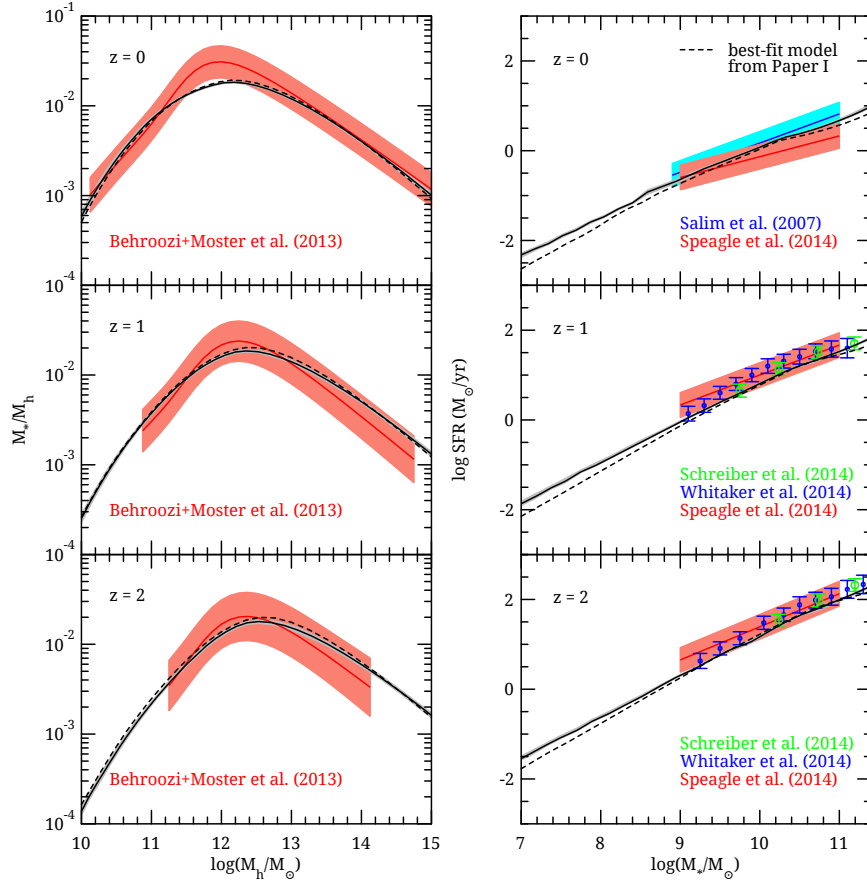


Figure 1. MCMC constraints on our first order equilibrium model for the stellar mass-halo mass relation (*left panel*) and the SFR- M_* relation (*right panel*) at $z = 0, 1, 2$. The solid black lines denote the best-fit model, whereas the thin gray shaded regions refer to their $1-\sigma$ confidence limits. All the errors on observed data sets, described in §2.1, indicate corresponding $1-\sigma$ uncertainties. The best-fit model from our Paper I is shown by dashed black lines for comparison.

to obtain the masses of individual halos that merge with a given halo of mass M . Each such sampling produces a discrete set of masses of halos that merge with a given parent halo of mass M . In details, we split the merger ratio integral of Equation 8 into two components: (i) *Merger component* - first we compute the probability (P_i) of a merger in some mass bins by summing up the integrand of Equation 8. If $P_i < 1$, we generate a uniform random number between $0 - 1$ and accept each merger with that probability only when P_i is greater than that random number. We stop this calculation once we get to the regime where the probability is greater than one. (ii) *Smooth component* - we do the normal integration down to ϵ_{\min} from the point where we stopped the previous calculation. Finally, adding up both components will give the total \dot{M}_h . We follow the same procedure for many different realizations and obtain an array of different accretion rates for a given M . In this manner, we obtain the the inflow rate including fluctuations owing to halo mergers.

We have implemented this into the equilibrium model and done an MCMC fit the mean scaling relations as was done in Paper I. This results in the fits previously shown in Figure 1, with the parameter constraints listed in Table 1. The fits are very similar to those arising from the first-order model.

3 RESULTS AND DISCUSSION

We now turn our attention to the main aim of this paper, namely to understand the origin of the scatter in the star-forming main sequence. We will assume that the fluctuations in the halo accretion rate are reflected directly in fluctuations in the star formation rate, as per equation 2. While it clearly takes some time for the halo inflow to reach the galaxy and form stars, we are assuming that once equilibrium is reached, the statistical variations are the same. To examine this in more detail, we begin by quantifying the fluctuations in \dot{M}_h .

3.1 Halo inflow rate fluctuations

Figure 2 displays the *total* variations in the accretion rate (\dot{M}_h) as a function of halo mass at $z = 0$ (*left panel*) and $z = 2$ (*right panel*). At a fixed halo mass, we get a range of accretion rates, denoted by gray points, owing to our random selection approach over 1000 trials. The average accretion rate in bins of M_h is denoted by the solid black line, which can be compared to the red line which is the smooth halo mass accretion rate we used in Paper I. On average, the halo accretion rate is well-represented by sampling the stochastic distribution.

For $z = 2$, the black curve is a very close match to the the first-order mean inflow rate, as most of growth is predominantly in the “smooth” mode (i.e. probability $P_i \gtrsim 1$). Towards lower redshifts,

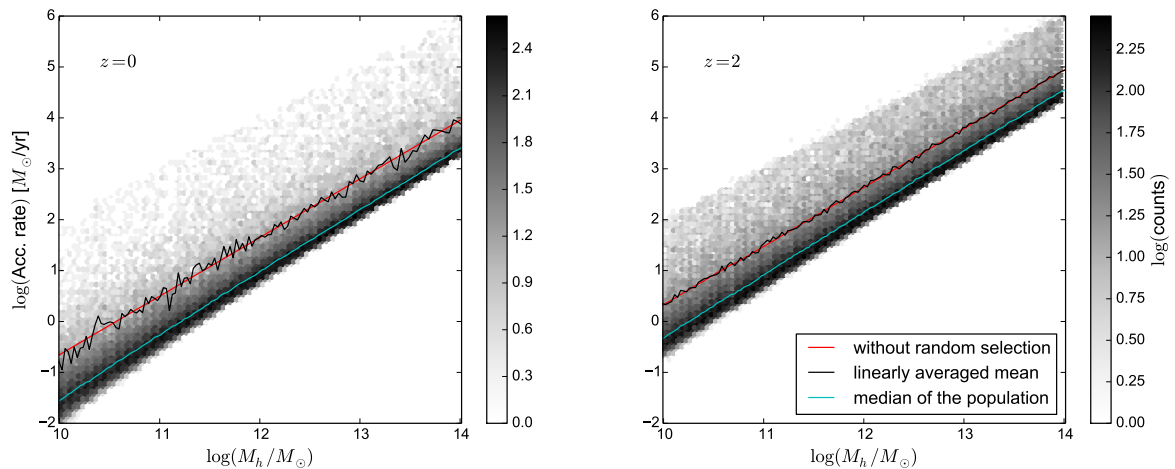


Figure 2. Total fluctuations in halo mass accretion rates at redshifts $z = 0$ and 2 for 1000 different realizations. The black and cyan curve represent respectively the linearly averaged mean and median of that distribution, whereas the red one denotes the accretion rates of the first order model.

the merger contribution from stochasticity becomes more significant, which is consistent with trends seen from hydrodynamic simulations (e.g. Kereš et al. 2005). The *median* of the population is shown here by the solid cyan line which lies towards the denser ends of \dot{M}_h -distribution as this quantity is less affected by extreme outliers than the mean¹.

Here we are interested in the scatter about this mean relation. The scatter appears to be fairly asymmetric, with a large tail to higher accretion rate owing to high mass ratio mergers. A more quantitative estimate of the scatter can be obtained by fitting a Gaussian or a double-Gaussian (Goerdts et al. 2015) to the histogram of that distribution; we will investigate this in the next section. We find that, although our resulting distribution of inflow rate seems skewed with a large tail, a single Gaussian fit turns out to be sufficient for our current purposes. The tail of the distribution corresponds to starbursts, which we will quantify later.

3.2 The scatter around the main sequence

To investigate how the scatter in M_* -SFR relation arises from stochasticity in the accretion rate, recall Equation 2 which directly relates the SFRs with the halo mass accretion rates (\dot{M}_{grav}). For this paper, we only investigate the scatter associated with halo inflow. It is also possible that there is scatter associated with some of the baryon cycling parameters; for instance the mass loading factor and preventive feedback may vary between galaxies at a fixed mass (Forbes et al. 2014). For simplicity, we do not consider these additional sources of scatter into our current analysis, rather we restrict ourselves to determine the main sequence scatter arising only from the dispersion in inflow rates. We further note that we are intrinsically making the assumption that inflow into the halo is instantaneously reflected in inflow into the ISM; this is of course not

true, but modulo a delay related to the infall time through the halo, the spectrum of halo inflow fluctuations should generally reflect the ISM inflow fluctuations. Finally, here we have estimated the SFR averaged over $dt = 100$ Myr, denoted SFR(100); we will consider other timescales in §3.6.

The *total* variation of the star-forming main sequence is shown in Figure 3. Again the linearly averaged mean agrees with the first order model, as expected due to large number of samples. The evolution of MS shows a shallower slope at high stellar masses at later epoch as an outcome of the slowly-decreasing quenching mass in our model (Gabor & Davé 2015; Mitra et al. 2015). This behavior is noted in observations as well (Whitaker et al. 2014).

Additionally, we have also plotted some example star formation histories, specific star formation rate $\text{sSFR}(z)$, showing the total scatter at $M_* = 5 \times 10^9 M_\odot$ in Figure 4. The $\text{sSFR}(z)$ is seen to be evolving strongly with redshifts following $\text{sSFR} \propto (1+z)^b$, which is again consistent with the observations (Whitaker et al. 2014; Johnston et al. 2015). Unsurprisingly, the linearly averaged mean (black curves) is found to be “bumpy” at lower z and then starts to become smooth and matches the red one at higher redshifts $z \gtrsim 2$. The observed data points shown here are from Speagle et al. (2014); Whitaker et al. (2014); Kurczynski et al. (2016). Note that, our model seems to underpredict the sSFR slightly at $z \approx 1-2$, which was also seen in Figure 1, but overall is in good agreement with the data within their observational uncertainties.

To get an estimated scatter in MS, one must fit the probability distribution function (PDF) of the SFR at some stellar mass and redshift. We have obtained the number density distribution of galaxies in six stellar mass bins spanning from $10^8 M_\odot$ to $10^{11} M_\odot$ as a function of their star formation rates at a range of redshift $0.5 \leq z \leq 4$. We fit Gaussians to these distributions to objectively identify the MS and its outliers, similar to the analysis done by Rodighiero et al. (2011) (but also see Sargent et al. 2012 for a double-Gaussian fit).

Figure 5 shows some typical distributions at redshift range $0.5 < z < 1$ and $1.5 < z < 2$, where we plotted the normalised PDFs of the logarithmic SFR for mass bins $9.5 < \log(M_*/M_\odot) < 10$ (left panels) and $10 < \log(M_*/M_\odot) < 10.5$ (right panels). The Gaussian fits with the standard deviations $\sigma \approx 0.2$ dex are dis-

¹ The reason for choosing mean over the median in our MCMC analysis is that the former quantity is more easy (and faster) to calculate. Also the mean (black curve) closely matches the smooth halo accretion rates from the simulation (without random selection, red curves), whereas median underestimates those. So these extreme outliers are also significant to capture the whole picture.

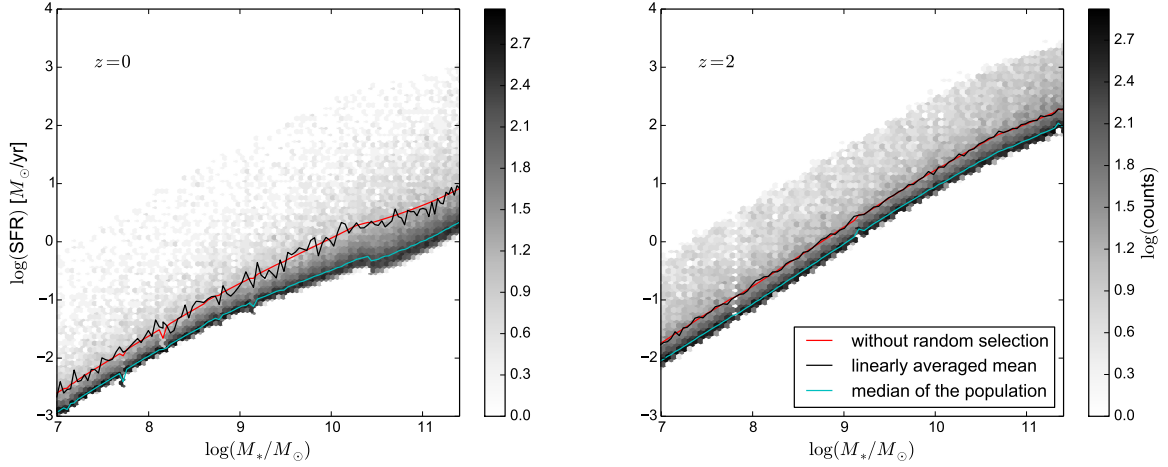


Figure 3. Same as Figure 2, but for the M_* -SFR relation.

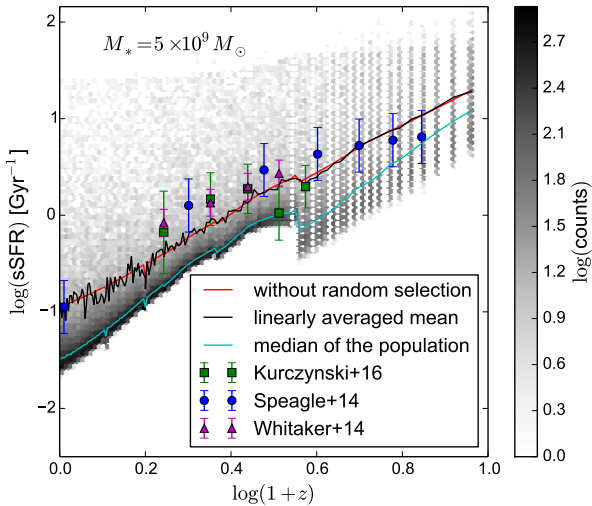


Figure 4. Total fluctuations in specific star formation rate as function of redshift at $M_* = 5 \times 10^9 M_\odot$. The absence of the lumpiness in linearly averaged mean curves (black) at earlier epoch corresponds to the halo growth in “smooth” mode.

played by the solid red curve. This log-normal fit in SFR is quite good over the bulk of the curve, but there is clearly an excess at high SFR; we will return to this in §3.5.

3.3 Comparison to previous observations and models

A key aim of this paper is to determine whether the simple equilibrium model can account for the observed scatter in the main sequence based on fluctuations in the inflow rate. To this end, we now compare our scatter predictions, along with their trends with galaxy mass and redshift, versus a range of recent observations. We also discuss comparisons to recent models and simulations that have predicted the MS scatter.

Figure 6 shows the estimated intrinsic scatters on the main se-

quence for all six stellar mass bins at various redshifts, computed as the width in dex of the log-normal fit. The individual values are presented in Table 2. Overall, we find that the standard deviation $\sigma_{\text{SFR}(100)}$ is $\sim 0.2 - 0.25$ dex, showing no significant trend with redshifts or stellar mass, except for a weak overall increase at higher redshifts.

Using the Spitzer MIPS observations, [Noeske et al. \(2007\)](#) and [Elbaz et al. \(2007\)](#) obtained a 0.3 dex scatter ($1-\sigma$) around the MS at $z \sim 1$, while [Whitaker et al. \(2012\)](#) reported a dispersion of 0.34 dex in the range $0 < z < 2.5$ using a sample of galaxies selected from the NEWFIRM Medium-Band Survey. Similarly, [Rodighiero et al. \(2011\)](#) determined a value of 0.24 dex scatter using mostly UV-derived SFRs. Recently, using the deep UV to NIR observations in the CANDELS fields, [Schreiber et al. \(2015\)](#) reported a scatter around the average SFR to be ~ 0.3 dex. These observational results refer to the total scatter, which includes observational measurement uncertainties. Several groups have attempted to correct for measurement errors to determine the intrinsic scatter. [Guo et al. \(2013\)](#) found intrinsic sSFR dispersions of 0.18 – 0.31 dex in the stellar mass range of $9.5 < \log(M_*/M_\odot) < 11.5$ at $z \sim 0.7$, while [Kurczynski et al. \(2016\)](#) found an intrinsic scatter of 0.2 to 0.4 dex in the redshift range $0.5 < z < 3$ and in the mass range $7 < \log(M_*/M_\odot) < 11$. Using the MOSDEF Survey of star-forming galaxies with $H\alpha$ and $H\beta$ spectroscopy, [Shivaei et al. \(2015\)](#) studied the MS relation at $z \sim 2$ and found an intrinsic scatter of ~ 0.31 dex for the SFR($H\alpha$) sample, which is 0.05 dex larger than what they measured from UV SFRs. [Speagle et al. \(2014\)](#) combined various measurements of the star-forming MS from literature by recalibrating them to use a common set of assumptions. After accounting for intrinsic scatter among SFR indicators, they found that the “true intrinsic” scatter is actually ~ 0.2 dex rather than the often reported 0.3 dex value and it remains roughly constant over cosmic time. Generally, observations tend to suggest a total scatter of 0.3 – 0.4 dex depending on mass and redshift, with the intrinsic scatter being as low as 0.2 dex.

The scatter we predict from the equilibrium model is overall in very good agreement with these observations. The model yields an intrinsic scatter of ~ 0.2 dex, with only a very slight mass dependence increasing to lower masses. We also don’t find a strong

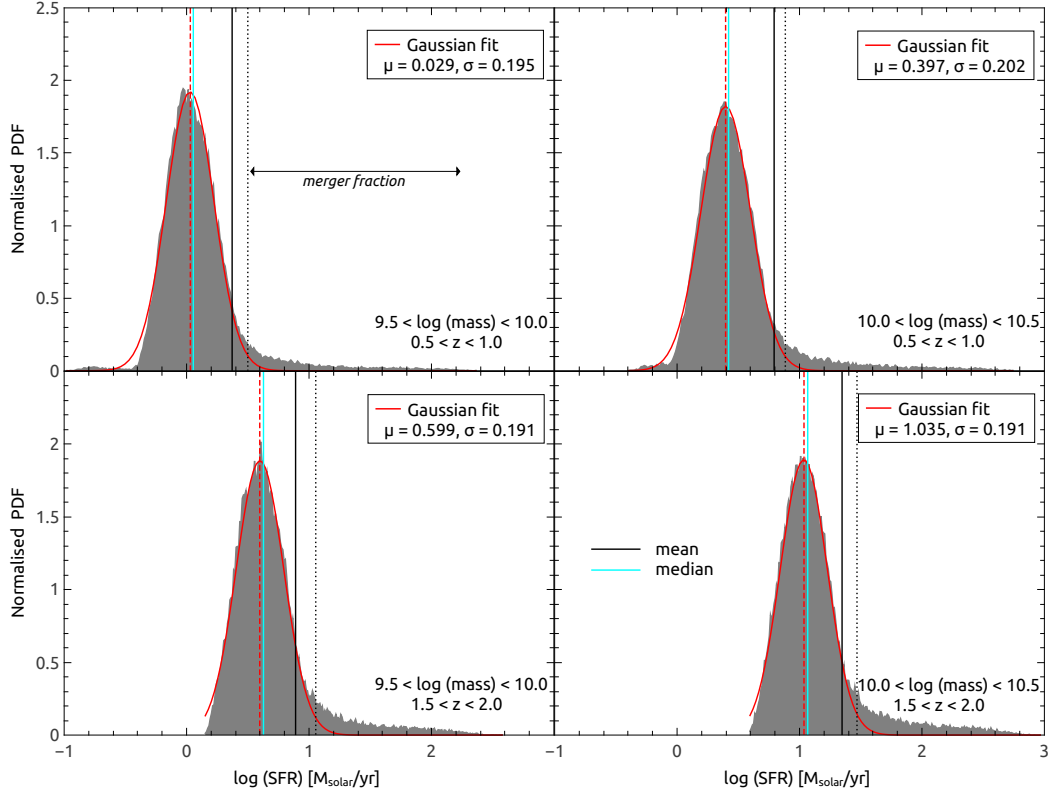


Figure 5. Normalised distributions (solid gray histograms) of SFRs in selected mass-redshift bins quoted in the figure. Shown in solid red curves are the individual Gaussian fits with a dispersion of ~ 0.2 dex to that distribution. Deviations (dotted black vertical lines) from the Gaussian are seen at $\sim 0.45 - 0.5$ dex (or 2.4σ) above the mean of the fits (dashed red vertical lines). The mean and median of those distributions are also shown here by solid black and cyan vertical lines respectively. Medians are found to be less affected by the extreme outliers at higher SFR ends and closely match the mode of the distributions, as expected.

| redshift range | $\sigma_{\text{SFR}(100)}$ [$\sigma_{\text{SFR}(30)}$] in dex | | | | | |
|---------------------|---|----------------------|----------------------|-----------------------|------------------------|------------------------|
| | $8 < \log M_* < 8.5$ | $8.5 < \log M_* < 9$ | $9 < \log M_* < 9.5$ | $9.5 < \log M_* < 10$ | $10 < \log M_* < 10.5$ | $10.5 < \log M_* < 11$ |
| $0.5 \leq z \leq 1$ | 0.203 [0.205] | 0.197 [0.202] | 0.199 [0.193] | 0.195 [0.199] | 0.202 [0.199] | 0.232 [0.266] |
| $1 < z \leq 1.5$ | 0.197 [0.216] | 0.191 [0.218] | 0.184 [0.223] | 0.177 [0.211] | 0.174 [0.204] | 0.173 [0.201] |
| $1.5 < z \leq 2$ | 0.206 [0.226] | 0.203 [0.222] | 0.195 [0.216] | 0.191 [0.225] | 0.191 [0.227] | 0.172 [0.207] |
| $2 < z \leq 2.5$ | 0.213 [0.290] | 0.208 [0.277] | 0.193 [0.289] | 0.220 [0.220] | 0.180 [0.210] | 0.155 [0.186] |
| $2.5 < z \leq 3$ | 0.244 [0.251] | 0.258 [0.296] | 0.252 [0.294] | 0.224 [0.305] | 0.207 [0.311] | 0.187 [0.275] |
| $3 < z \leq 3.5$ | 0.254 [0.313] | 0.248 [0.305] | 0.248 [0.307] | 0.240 [0.304] | 0.240 [0.301] | 0.203 [0.282] |
| $3.5 < z \leq 4$ | 0.250 [0.285] | 0.256 [0.317] | 0.255 [0.308] | 0.256 [0.298] | 0.241 [0.285] | 0.216 [0.296] |

Table 2. Intrinsic scatter around the main sequence of galaxies in bins of different stellar masses and redshifts averaged over timescale 100 Myr [30 Myr]. Typically, the scatter increases when we decrease the timescale. Overall, the $1-\sigma$ dispersion of $\sim 0.2 - 0.25$ dex for the 100 Myr case (or $\sim 0.2 - 0.3$ dex for 30 Myr) is broadly comparable with various recent observations.

redshift dependence out to $z \sim 2$, though it increases at all masses at $z \gtrsim 2.5$.

There are indications, particularly from (Kurczynski et al. 2016), that the intrinsic scatter may be significantly higher than 0.2 dex in some cases. Remember that our current approach only includes scatter associated with inflow fluctuations, while in principle there could be intrinsic variations in the mass outflow rate (η) or in preventive feedback (ζ), which would give extra scatter to the overall σ_{SFR} . Nonetheless, it is interesting that the lowest measured intrinsic scatters are quite consistent with our prediction

just from inflow fluctuations. This limits the stochasticity in outflows to relatively modest values, and suggests that galactic outflows must be a fairly steady phenomenon at least when averaged over ~ 100 Myr. Alternatively, there may be some relationship between outflow rates and inflow stochasticity such that a relatively tight correlation is maintained owing to correlated scatter.

Numerous galaxy evolution simulations and semi-analytical or analytical models have likewise made predictions for the intrinsic scatter around the M_* -SFR relation. Sparre et al. (2015b) used the Illustris simulation to obtain a $\sim 0.2 - 0.25$ dex scatter for

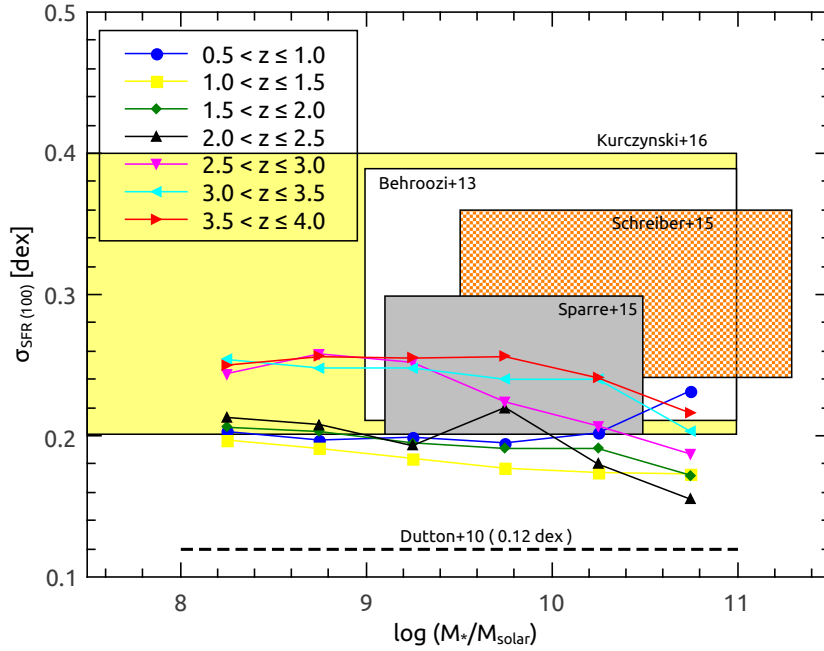


Figure 6. The main sequence scatter ($1\text{-}\sigma$) at redshift range $0.5 \leq z \leq 4$. In all cases, we estimate the SFR averaged over 100 Myr. For comparison, we show the typical scatter obtained from observations by [Schreiber et al. \(2015\)](#) (shaded orange bands) and [Kurczynski et al. \(2016\)](#) (shaded yellow; intrinsic scatter of 0.2 – 0.4 dex). For models, we show the Illustris simulation results ([Sparre et al. 2015b](#)) and results from the abundance matching models of [Behroozi et al. \(2013, see their Table 9\)](#) by the shaded gray and empty middle bands respectively. The prediction from the analytic disk model of [Dutton et al. \(2010\)](#) is shown as the dashed black line.

$M_* \lesssim 10^{10.5} M_\odot$, while the semi-analytic model for disk galaxy evolution by [Dutton et al. \(2010\)](#) predicted a lower scatter of 0.12 dex in SFR. Note that, this value is much less than the observed one as the later is likely to be dominated by observational uncertainties. However, this might also reflect the fact that [Dutton et al. \(2010\)](#) underestimated the true scatter due to their simplified treatment of the halo mass accretion history and thus additional sources of intrinsic scatter are probably required in their model. Using zoom-in hydro-cosmological simulations of massive galaxies at $z > 1$, [Tacchella et al. \(2016\)](#) examined the evolution of SFGs across the MS through gas *compaction, depletion* and *replenishment* and measured a *true* scatter of ~ 0.27 dex with a slightly increasing trend towards lower redshifts. Note that, if these processes are independent of inflow fluctuations, then these would contribute additional scatter around the MS. Recently, [Rodríguez-Puebla et al. \(2016\)](#) has reported a σ to be $\sim 0.35 - 0.45$ dex from a simple analytical approach based on the crucial assumption that the stellar-to-halo mass ratio is nearly independent of redshift up to $z \sim 4$. In general, our numbers are similar to that obtained from Illustris, which supports the notion that MS fluctuations in hydrodynamic simulations are arising from inflow stochasticity. The analytic models, on the other hand, have more widely varying predictions; this may owe to the fact that some of their assumptions may not be reflective of how galaxy formation proceeds via baryon cycle-driven growth.

Our method is quite similar in many ways to that in [Forbes et al. \(2014\)](#), who examine the scatter in the main sequence as well as in the MZR and FMR arising from the scatter in dark matter accretion rates as well as some of the baryon cycling parameters from their bathtub model. Considering a typical N-body predicted stochastic scatter in the accretion rates, they found that the scatter in both the MS and MZR at fixed stellar mass is comparable to or larger than the observed ones and roughly independent of halo mass

and redshift. Although we compute stochasticity in a different way and use a full MCMC approach to characterise the best-fit relations, we echo their general conclusion that fluctuations in feedback parameters must be sub-dominant.

3.4 Mass and redshift dependence of the scatter

The mass and redshift dependence of the MS scatter has also been a subject of some debate. Cosmological models like Illustris generally predict a constant scatter to low masses ([Sparre et al. 2015b](#)), although this simulation predicts a growing scatter at high masses as quenched galaxies enter into their sample. In contrast, the FIRE simulations analysed by [Sparre et al. \(2015a\)](#) finds that $M_* \sim 10^9 M_\odot$ galaxies can have extremely bursty SFHs, with a scatter well over 0.5 dex on short timescales, and argued this owed to their high resolution and more self-consistent implementation of feedback processes.

Observations are also starting to characterise the mass dependence of the MS scatter. Results from [Rodighiero et al. \(2011\)](#), [Whitaker et al. \(2012\)](#), and [Schreiber et al. \(2015\)](#), generally found the scatter to be independent of M_* , and also z , down to M_* as low as $\sim 10^{9.5} M_\odot$ at various epochs. Also, [Rodríguez-Puebla et al. \(2016\)](#) did not notice a clear trend with mass to even lower masses.

In the equilibrium model, the scatter arises purely from halo inflow fluctuations. Since halo mass growth rates are fairly self-similar, one doesn't expect a strong trend with halo mass, and thus stellar mass, in the scatter. Hence it is expected that our scatter has only a very weak mass dependence, which is what we see in [Figure 6](#). This seems to be broadly in agreement with observations, which again supports the notion that SFR fluctuations are primarily driven by inflow fluctuations. In the case of FIRE, the larger scat-

ter is likely driven by the strong variations in outflow strength on small timescales in dwarf galaxies; as observations of such galaxies improves, this will provide a significant constraint how bursty low-mass galaxy SFHs can be.

We also find no redshift dependence in the scatter up to $z \sim 2$, and then a modest increase at higher redshifts. This is in agreement with observations by Kurczynski et al. (2016) who also found essentially no evolution in intrinsic scatter, with a typical value of $\sigma \sim 0.25$ from $z \sim 1 - 3$. They did find a higher scatter at $z \lesssim 1$, which likely owes to the inclusion of galaxies on their way to being quenched. Meanwhile, our results are in agreement with the model by Rodríguez-Puebla et al. (2016) who averaged the halo accretion rate over the dynamical timescale and found no redshift dependence. Overall, the predicted lack of a strong redshift dependence seems consistent with available data.

In summary, the equilibrium model predicts SFR scatter at a given M_* that is comparable to the lowest values for the observed intrinsic scatter, and are generally below observed values for the total scatter. Models show a larger range in scatter depending on assumptions and techniques, but the equilibrium model predictions generally agrees most closely with predictions taken directly from cosmological hydrodynamic simulations. We do not find a strong mass or redshift dependence in the scatter, suggesting that dwarf/early galaxy SFHs are not expected to be significantly burstier. This is generally in agreement with available data, and bolsters our claim that halo inflow fluctuations, which are expected to be fairly self-similar with mass, drive SFR fluctuations.

3.5 Merger-driven starbursts

Not all galaxies lie within the scatter of the main sequence. Galaxies fall below the main sequence as they are quenched by a variety of processes such as black hole feedback or gas stripping processes (Somerville & Davé 2015). The outliers above the main sequence are starburst galaxies, and can be identified in our model as high upwards fluctuations in the inflow rate. Even though the equilibrium model does not account for internal dynamical processes that can drive the most extreme starbursts (Mihos & Hernquist 1996; Sanders & Mirabel 1996), such galaxies are very rare and require special initial conditions, while more typical mergers are far less extreme (Cox et al. 2008). We can thus quantify in our model the fraction of galaxies in such mergers, as well as their global contribution to overall star formation.

We quantify the merger-induced fraction of SFR by computing the excess SFR owing to mergers from each histogram in Figure 7. To compare with data, we adopt a cut of $\sim 0.45 - 0.5$ dex (or 2.4σ) above the MS (vertical dotted line), and declare the fraction of SFR occurring above this to be merger-induced; this is analogous to the procedure done in observations by Rodighiero et al. (2011). The resulting values are very similar to that obtained by directly summing the difference between the histograms and the best-fit Gaussians in Figure 5.

Figure 7 shows that the amount of merger-induced SF is generally quite small, around $\sim 5 - 15\%$, at all epochs out to $z \sim 2.5$. There is a mild trend for an increase in merger-induced SF towards higher redshifts. Since these galaxies are contributing disproportionately to the SFR relative to their numbers, the fraction of galaxies that lie in this merger regime is even smaller.

Our predicted values are quite consistent with the observational determination by Rodighiero et al. (2011), at the relevant redshift $z \sim 2$. Also we do not predict a strong mass dependence, which is also generally consistent with these data. Interestingly, we

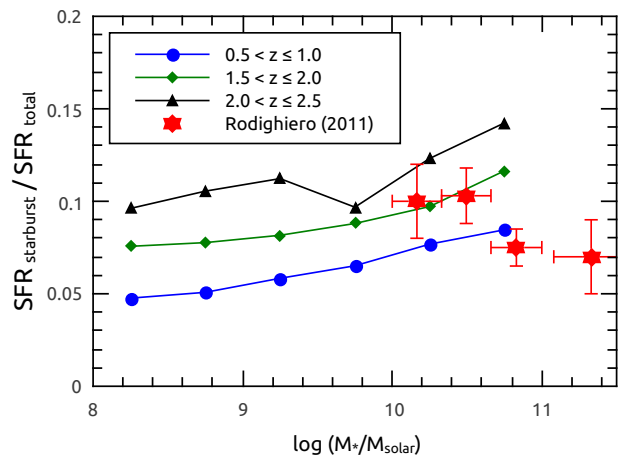


Figure 7. Contribution of starburst galaxies (2.4σ above the MS) to the total SFR as a function of stellar mass at different redshift bins. The observed Rodighiero et al. (2011) data sets (red points with error bars) at $1.5 < z < 2.5$ are also plotted for comparison.

predict a weak increase in merger-induced SF to higher masses, which is expected because halo mergers are increasingly important at high halo masses (Guo & White 2008). The data if anything seem to favor an anti-correlation with mass, but the dynamic range is not yet large enough to make conclusive statements. There are, however, some observational indications of bursty star formation at lower masses on timescales much less than ~ 100 Myr (Weisz et al. 2012; Kauffmann 2014; Guo et al. 2016). Even though these bursty population of low-mass galaxies can contribute as much as 50 – 60% to their present-day mass (Kauffmann 2014), the equilibrium model does not predict any such trend.

Overall, during the peak activity of cosmic star formation until today, galaxy growth in our equilibrium model is strongly dominated by galaxies lying within the Gaussian scatter around the main sequence. This conclusion is consistent with currently available observations, as well as longstanding predictions from cosmological simulations (Murali et al. 2002; Kereš et al. 2005). This motivates the idea that merger-induced star formation represent a second-order effect in global galaxy growth, while the primary driver remains steady (but mildly fluctuating) gravitational inflow.

3.6 Timescale variability in SFRs

So far, we have estimated the dispersion in MS using the SFRs averaged over 100 Myr. However, the inferred SFRs of galaxies are sensitive to the choice of timescale over which the SFR is averaged. (Kennicutt & Evans 2012; Hopkins et al. 2014; Sparre et al. 2015b). $H\alpha$ tends to measure star formation traced by the most massive stars hence and fluctuations on scales of tens of Myr, while UV-based measures tend to trace somewhat less massive (OB) stars with timescales of ~ 100 Myr. Far-infrared measures come from dust-reprocessed light which can trace even longer timescales. Hence it is interesting to measure the scatter in SFR smoothed over different time intervals.

Figure 8 shows the SFR scatter averaged over 30 Myr (also see Table 2) and 300 Myr, along with our canonical value of 100 Myr, for two different redshift ranges: $0.5 < z \leq 1$ (circle) and $3.5 < z \leq 4$ (right triangle). Generally, the scatter decreases when we

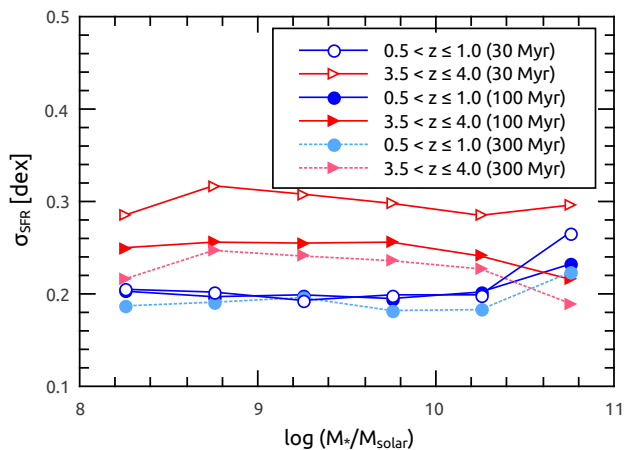


Figure 8. Scatter in main sequence with the SFR averaged over different timescales (30, 100 and 300 Myr). Overall, the dispersion increases for shorter timescale variability and declines for longer timescales.

increase the timescale, which is expected as the SFHs of galaxies are essentially smoothed out for longer timescale variability. This is qualitatively in agreement with other studies (Hopkins et al. 2014; Sparre et al. 2015b).

In detail, at low redshifts the differences among timescales are fairly negligible. This is expected because the accretion timescales at late epochs are quite long. Meanwhile, at high redshifts there is a very clear trend, with 30 Myr scatter being ≈ 0.3 dex as opposed to longer timescale scatter being ≈ 0.25 dex. Still, all these variations are rather modest. Hence the equilibrium model does not predict that short timescale SFR indicators such as H α will display significantly greater scatter. It remains to be seen if this is in agreement with observations.

4 SUMMARY

The equilibrium model for galaxy evolution highlights galactic inflows and outflows as the main governor of galaxy growth, in accord with the emerging baryon cycling paradigm for galaxy self-regulation. Using a Bayesian Monte Carlo Markov chain approach, we showed in Paper I that our baryon cycling-based model can match observed mean galaxy scaling relations across the majority of cosmic time better and with many fewer parameters than in traditional merger-tree based semi-analytic models.

In this work, we test the basic equilibrium model by capturing the “second-order” galaxy evolutionary processes i.e. the deviations from these mean trends, which we assume here are driven by the fluctuations in the inflow rate, including mergers. The goal is to understand the origin of the scatter in the scaling relation between the stellar mass and the star formation rate (known as the main sequence), and quantify the contribution from the scatter in mean dark matter accretion rates.

We introduce a novel approach to incorporate fluctuations in the inflow rates by sampling the merger rates derived from N-body simulations. Assuming that such dark matter fluctuations in halo accretion are proportionally translated into baryonic inflow fluctuations into the galaxy, we make predictions for the scatter around the star forming galaxy main sequence. We calculate the 1- σ scatter within stellar mass bins spanning from $8 < \log(M_*/M_\odot) < 11$

for different redshift ranges, by fitting a Gaussian to the log of the SFR distribution (i.e. a log-normal). Although the distributions of log SFR are somewhat skewed with an excess tail towards large SFR, they can still be reasonably described by a single Gaussian fit (Rodighiero et al. 2011) that encloses the MS. The tail portion corresponds to the starburst regime. We average over several different timescales to estimate how the scatter would change amongst different SFR indicators. In this way, we quantify the intrinsic MS scatter as a function of mass, redshift, and timescale.

Our main findings are summarized as follows:

- With a sufficiently large number of realizations, we show that the linearly averaged mean of that inflow rate distribution closely follows our the smooth accretion rate we assumed in Paper I. Hence we confirm that our stochastic approach closely reproduces the results from our first-order model in Paper I. For higher redshifts, they are almost identical as we enter a regime of smooth accretion mode, while to lower redshifts the contribution from mergers grows (though is still sub-dominant).
- The merger-based inflow fluctuations translate into a significant intrinsic scatter in the star-forming main sequence of $\approx 0.2 - 0.25$ dex. This is generally somewhat lower than observed values of the scatter which include measurement error, and is comparable to the lowest values when observations attempt to infer the intrinsic scatter by subtracting off measurement error. Interestingly, our reported value is in excellent agreement with the results from Speagle et al. (2014) where they compile various observed data sets and find the true scatter in MS, after correcting for the observation-induced errors, to be ~ 0.2 dex rather than ~ 0.3 dex. This highlights our primary result, that fluctuations in the dark matter accretion rate are the primary driver of the observed MS scatter.
- We predict very little dependence on stellar mass in the scatter down to $M_* = 10^9 M_\odot$. this trend is broadly in agreement with observational studies (Whitaker et al. 2012; Schreiber et al. 2015; Rodríguez-Puebla et al. 2016; Kurczynski et al. 2016). It is also generally consistent with hydrodynamic simulations, but is less consistent with the higher-resolution FIRE simulations that show must burstier star formation at low masses owing to a duty cycle set up by intermittent strong feedback. If such burstiness is eventually confirmed in observations, it would suggest that we must include variability in our mass outflow rate η at low masses into our equilibrium model. Currently, however, most of the observations do not conclusively favour this (but also see Weisz et al. 2012; Kauffmann 2014; Guo et al. 2016).
- We predict that the MS scatter has only minimal redshift dependence, increasing slightly at high redshifts. We also show that at later epochs, the scatter is mostly independent of SFR timescale, while at early epochs it increases modestly to shorter timescales.
- The contribution to the global SFR from merger-induced star formation is minimal at all explored redshifts, typically 5 – 15% with a mild trend towards being higher at high redshifts. Hence starbursts are strongly sub-dominant in terms of overall stellar growth in our models. This is consistent with available observations and cosmologically-situated models.

Our results indicate that we have successfully tested the equilibrium model by predicting scatter around the main sequence purely from inflow fluctuations, and that such fluctuations are the primary driver for deviations from the main sequence.

In this work we have not considered fluctuations in the baryon cycling parameters. Potentially, one could use the scatter in the mass-metallicity relation to constrain this. In the absence of recycling, the mass dependence of the metallicity is purely set by that

of η , so in principle the mass-metallicity scatter constrains the η scatter. But one could likely also introduce scatter in ζ and/or t_{rec} to achieve a similar result. Satellites also deviate systematically in metallicity from central galaxies, so we are engaged in developing models to incorporate satellite stripping processes in order to quantify their contribution to the MS scatter (Simha et al., in preparation). Still, given that the scatter in mass-metallicity is typically quite small (~ 0.1 dex), this suggests that inflow fluctuations will continue to dominate the MS scatter.

The equilibrium model is developing into a valuable and intuitive tool to study galaxy evolution within a simple baryon cycling framework. In a sense, this model is starting down the road to “precision galaxy formation”, in which the first-order parameters that establish galaxy growth can start to be constrained by observations, in analogy with the main parameters in precision cosmology. Meanwhile, other processes such as galaxy mergers represent second-order effects to global galaxy growth, and impact a different set of observables such as galaxy morphological transformations and satellite-specific processes. Incorporating halo mergers in a probabilistic fashion as we have done here is a key step towards extensions of the equilibrium model that will develop this tool into a leading platform for understanding galaxy evolution within a baryon cycling framework.

ACKNOWLEDGEMENTS

SM, RD, and VS acknowledge support from the South African Research Chairs Initiative and the South African National Research Foundation. Support for RD was also provided by NASA ATP grant NNX12AH86G to the University of Arizona.

REFERENCES

- Andrews B. H., Martini P., 2013, *ApJ*, **765**, 140
- Balogh M. L., Pearce F. R., Bower R. G., Kay S. T., 2001, *MNRAS*, **326**, 1228
- Behroozi P. S., Wechsler R. H., Conroy C., 2013, *ApJ*, **770**, 57
- Bouché N., et al., 2010, *ApJ*, **718**, 1001
- Boylan-Kolchin M., Springel V., White S. D. M., Jenkins A., Lemson G., 2009, *MNRAS*, **398**, 1150
- Christensen C. R., Davé R., Governato F., Pontzen A., Brooks A., Munshi F., Quinn T., Wadsley J., 2016, *ApJ*, **824**, 57
- Cox T. J., Jonsson P., Somerville R. S., Primack J. R., Dekel A., 2008, *MNRAS*, **384**, 386
- Daddi E., et al., 2007, *ApJ*, **670**, 156
- Davé R., Oppenheimer B. D., Finlator K., 2011, *MNRAS*, **415**, 11
- Davé R., Finlator K., Oppenheimer B. D., 2012, *MNRAS*, **421**, 98
- Davé R., Thompson R., Hopkins P. F., 2016, *MNRAS*, **462**, 3265
- Dekel A., Mandelker N., 2014, *MNRAS*, **444**, 2071
- Dekel A., et al., 2009, *Nature*, **457**, 451
- Di Cintio A., Brook C. B., Macciò A. V., Stinson G. S., Knebe A., Dutton A. A., Wadsley J., 2014, *MNRAS*, **437**, 415
- Dutton A. A., van den Bosch F. C., Dekel A., 2010, *MNRAS*, **405**, 1690
- Elbaz D., et al., 2007, *A&A*, **468**, 33
- Fakhouri O., Ma C.-P., Boylan-Kolchin M., 2010, *MNRAS*, **406**, 2267
- Finlator K., Davé R., 2008, *MNRAS*, **385**, 2181
- Forbes J. C., Krumholz M. R., Burkert A., Dekel A., 2014, *MNRAS*, **443**, 168
- Gabor J. M., Davé R., 2015, *MNRAS*, **447**, 374
- Genel S., et al., 2014, *MNRAS*, **445**, 175
- Goerdt T., Ceverino D., Dekel A., Teyssier R., 2015, *MNRAS*, **454**, 637
- Guo Q., White S. D. M., 2008, *MNRAS*, **384**, 2
- Guo K., Zheng X. Z., Fu H., 2013, *ApJ*, **778**, 23
- Guo Y., et al., 2016, preprint, ([arXiv:1604.05314](https://arxiv.org/abs/1604.05314))
- Henriques B. M. B., White S. D. M., Thomas P. A., Angulo R. E., Guo Q., Lemson G., Springel V., 2013, *MNRAS*, **431**, 3373
- Hopkins P. F., Kereš D., Oñorbe J., Faucher-Giguère C.-A., Quataert E., Murray N., Bullock J. S., 2014, *MNRAS*, **445**, 581
- Johnston R., Vaccari M., Jarvis M., Smith M., Giovannoli E., Häußler B., Prescott M., 2015, *MNRAS*, **453**, 2540
- Kauffmann G., 2014, *MNRAS*, **441**, 2717
- Kennicutt R. C., Evans N. J., 2012, *ARA&A*, **50**, 531
- Kereš D., Katz N., Weinberg D. H., Davé R., 2005, *MNRAS*, **363**, 2
- Krumholz M. R., Dekel A., 2012, *ApJ*, **753**, 16
- Kurczynski P., et al., 2016, *ApJL*, **820**, L1
- Lilly S. J., Carollo C. M., Pipino A., Renzini A., Peng Y., 2013, *ApJ*, **772**, 119
- Martin C. L., 2005, *ApJ*, **621**, 227
- Mihos J. C., Hernquist L., 1996, *ApJ*, **464**, 641
- Mitra S., Davé R., Finlator K., 2015, *MNRAS*, **452**, 1184
- Mo H. J., Mao S., White S. D. M., 1998, *MNRAS*, **295**, 319
- Moster B. P., Naab T., White S. D. M., 2013, *MNRAS*, **428**, 3121
- Murali C., Katz N., Hernquist L., Weinberg D. H., Davé R., 2002, *ApJ*, **571**, 1
- Muratov A. L., Kereš D., Faucher-Giguère C.-A., Hopkins P. F., Quataert E., Murray N., 2015, *MNRAS*, **454**, 2691
- Noeske K. G., et al., 2007, *ApJL*, **660**, L43
- Oppenheimer B. D., Davé R., Kereš D., Fardal M., Katz N., Kollmeier J. A., Weinberg D. H., 2010, *MNRAS*, **406**, 2325
- Peng Y.-j., Maiolino R., 2014, *MNRAS*, **443**, 3643
- Planck Collaboration et al., 2015, preprint, ([arXiv:1502.01589](https://arxiv.org/abs/1502.01589))
- Rodighiero G., et al., 2011, *ApJL*, **739**, L40
- Rodríguez-Puebla A., Primack J. R., Behroozi P., Faber S. M., 2016, *MNRAS*, **455**, 2592
- Rubin K. H. R., Prochaska J. X., Koo D. C., Phillips A. C., Martin C. L., Winstrom L. O., 2014, *ApJ*, **794**, 156
- Saintonge A., et al., 2013, *ApJ*, **778**, 2
- Salim S., et al., 2007, *ApJS*, **173**, 267
- Sanders D. B., Mirabel I. F., 1996, *ARA&A*, **34**, 749
- Sanders R. L., et al., 2015, *ApJ*, **799**, 138
- Sargent M. T., Béthermin M., Daddi E., Elbaz D., 2012, *ApJL*, **747**, L31
- Schaye J., et al., 2015, *MNRAS*, **446**, 521
- Schreiber C., et al., 2015, *A&A*, **575**, A74
- Shivaei I., et al., 2015, *ApJ*, **815**, 98
- Somerville R. S., Davé R., 2015, *ARA&A*, **53**, 51
- Sparre M., Hayward C. C., Feldmann R., Faucher-Giguère C.-A., Muratov A. L., Kereš D., Hopkins P. F., 2015a, preprint, ([arXiv:1510.03869](https://arxiv.org/abs/1510.03869))
- Sparre M., et al., 2015b, *MNRAS*, **447**, 3548
- Speagle J. S., Steinhardt C. L., Capak P. L., Silverman J. D., 2014, *ApJS*, **214**, 15
- Springel V., et al., 2005, *Nature*, **435**, 629
- Steidel C. C., Erb D. K., Shapley A. E., Pettini M., Reddy N., Bogosavljević M., Rudie G. C., Rakic O., 2010, *ApJ*, **717**, 289
- Steidel C. C., et al., 2014, *ApJ*, **795**, 165
- Tacchella S., Dekel A., Carollo C. M., Ceverino D., DeGraf C., Lapiner S., Mandelker N., Primack Joel R., 2016, *MNRAS*, **457**, 2790
- Tacconi L. J., et al., 2013, *ApJ*, **768**, 74
- Tremonti C. A., et al., 2004, *ApJ*, **613**, 898
- Weiner B. J., et al., 2009, *ApJ*, **692**, 187
- Weisz D. R., et al., 2012, *ApJ*, **744**, 44
- Wetzel A. R., Hopkins P. F., Kim J.-h., Faucher-Giguère C.-A., Kereš D., Quataert E., 2016, *ApJL*, **827**, L23
- Whitaker K. E., van Dokkum P. G., Brammer G., Franx M., 2012, *ApJL*, **754**, L29
- Whitaker K. E., et al., 2014, *ApJ*, **795**, 104
- White S. D. M., Frenk C. S., 1991, *ApJ*, **379**, 52
- Zahid H. J., Dima G. I., Kudritzki R.-P., Kewley L. J., Geller M. J., Hwang H. S., Silverman J. D., Kashino D., 2014, *ApJ*, **791**, 130